Silicon-based Fano resonance devices based on photonic crystal nanobeams*

WANG Yihao[1], LU Wenda[2], LAI Xiaohan[2], DONG Mingli[1], LU Lidan[1], and ZHU Lianqing[1]**

1. Beijing Information Science and Technology University, Beijing 100192, China

2. State Grid Zhejiang Electric Power Corporation Information & Telecommunication Branch, Hangzhou 310007, China

(Received 11 April 2023; Revised 18 May 2023)

To address the driving power and density of wavelength-division-multiplexing (WDM) computing architectures, a Fano resonator based on a photonic crystal nanobeam is proposed. The Fano resonator comprises a T-shaped waveguide, introducing an additional phase shift in the continuous propagation mode, and a photonic crystal nanobeam with a discrete mode. The device has one resonance peak within wavelength ranging from 1 500 nm to 1 600 nm, with a maximum extinction ratio of 8.7 dB and a transmission spectrum slope of up to 11.30 dB/nm. The device has good reusability, extinction ratio, and spectral resolution. It is expected to provide essential photonic components for low-energy consumption and high-density photonic computing to meet the requirements of future convolutional neural network (CNN) acceleration computing.

Document code: A **Article ID:** 1673-1905(2023)12-0727-5

DOI https://doi.org/10.1007/s11801-023-3067-0

In recent years, convolutional neural networks (CNNs) have achieved great success in various fields, such as computer vision, image, and speech processing[1,2]. However, its advantages cannot be exerted without the support of hardware accelerators. Due to the electronic device's power and speed limitations, current electronic accelerators cannot meet the hardware computing power and energy consumption requirements for future large-scale convolution operations[3,4]. Photon accelerators have advantages that electronic components do not have such as high bandwidth, low power consumption, and electromagnetic interference resistance[5].

It is theoretically possible to multiplex several hundred high-speed information channels with a single silicon photonic waveguide by encoding each channel with a different wavelength. This approach is called wavelength division multiplexing (WDM)[6,7]. WDM can be achieved through micro-ring resonators (MRRs) and photonic crystal nanobeam modulators[8,9]. WDM maximizes photonics parallelism and increases the throughput of the information process. However, MRRs have multiple resonant peaks and are susceptible to channel crosstalk, which reduces the multiplexing efficiency. Photonic crystal nanobeam structures are compact and have no free spectral range (*FSR*) in a wide wavelength band, making them less susceptible to channel crosstalk and more suitable for future large-scale integrated photonics devices[10-13]. In Ref.[10], a photon convolution accelerator called HolyLight is proposed based on MRR. The framework uses MRR for convolution operations and composes a 128×128 optical matrix multiplication array to perform parallel processing of data, effectively increasing throughput, but it still has channel crosstalk issues. Ref.[11] proposes a photonic crystal nanobeam cavity (PCNC) convolutional pool accelerator that utilizes the feature of PCNC without *FSR* in the C band for large-scale multiplexing, making it suitable for even larger-scale computations. However, the spectral resolution of its photonic crystal is low. Ref.[12] is stated that the interference between the high-order leaky mode in the optical waveguide and the one-dimensional topological protected boundary state can be utilized to form the Fano resonance. Due to the sharp, asymmetric resonant peaks of the Fano line shape, the spectral resolution can be further improved. However, the slope of the Fano resonant peak in this method is only 10 dB/nm and the structure is relatively complex.

This paper proposes a structure for a T-waveguide-coupled PCNC that addresses the abovementioned shortcomings. The Fabry-Perot (FP) cavity generated by the T-waveguide is used as a continuous state. The PCNC provides a discrete state. The impact of device structure parameters on device performance was analyzed using the finite-difference time-domain (FDTD) method in the

* This work has been supported by the Science and Technology Project of the State Grid Zhejiang Electric Power Company Limited (No.B311XT21004G).

** E-mail: dongml@bistu.edu.cn

Lumerical simulation platform. The device exhibits excellent performance with a high extinction ratio and high contrast by optimizing the structural parameters.

Fig.1 shows a side-coupled photonic crystal nanobeam structure, where the T-waveguide is coupled with the photonic crystal. The complete waveguide structure is constituted by a hybrid of an S-bend waveguide and a T-waveguide. Light is injected from the input port of the waveguide, passes through a resonant cavity, and is ultimately output from the waveguide's output port. Firstly, the device is theoretically analyzed, and according to the temporal coupled-mode theory (TCMT)[14], it can be concluded that

$$\mathrm{i}\omega A = \mathrm{i}\omega_0 A - A\tau_a - A\tau_r + \sqrt{2\tau_r}S_{I+}, \tag{1}$$

$$S_{I-} = S_{I+} - \sqrt{2\tau_r}A, \tag{2}$$

$$S_{R-} = \sqrt{2\tau_a}A, \tag{3}$$

where A represents the amplitude of the nanobeam cavity resonance mode, S_{I+}, S_{I-}, and S_{R-} represent the input, output, and reflected amplitudes. ω_0 is the resonant frequency. τ_a is the amplitude coupling coefficient between the PCNC and the input end of the bus waveguide, while τ_r is the amplitude coupling coefficient between the PCNC and the output end of the bus waveguide. Ignoring radiation losses for any frequency, the sum of the spectral transmittance and reflectance satisfies the energy conservation law. Thus, the normalized spectral transmission is always equal to 1. By solving Eqs.(1)—(3), the transmittance expression can be obtained as

$$T(\omega) = \left|\frac{S_{I-}}{S_{I+}}\right|^2 = \frac{(\omega-\omega_0)^2 + (\tau_r-\tau_a)^2}{(\omega-\omega_0)^2 + (\tau_r+\tau_a)^2}. \tag{4}$$

Since the structure is entirely centrosymmetric, it follows that τ_a=τ_r=τ. Therefore,

$$T(\omega) = \left|\frac{S_{I-}}{S_{I+}}\right|^2 = \frac{(\omega-\omega_0)^2}{(\omega-\omega_0)^2 + 4\tau^2}. \tag{5}$$

From Eq.(5), the theoretical transmittance spectrum of the side-coupled structure can be obtained, which depicts a Lorentzian line shape, as shown in Fig.2. In the ideal case where the radiation loss rate is very low and can be neglected, when the frequency of the incident light is identical to the resonant frequency of the cavity (i.e., ω=ω_0), the transmittance is 0.

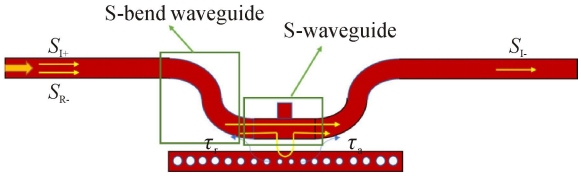

Fig.1 Side-coupled photonic crystal nanobeam structures

To transform the Lorentzian resonance line shape of the PCNC into an asymmetric Fano line shape, it is necessary to change the phase difference between the discrete and continuous states. However, it cannot be an integer multiple of 2π. Therefore, this paper proposes a PCNC-coupled T-shaped waveguide structure, which adds a rectangular waveguide to the bus waveguide in the coupling region, as shown in Fig.1. The T-shaped waveguide can induce an additional phase shift on the continuous propagation mode in the bus waveguide. Moreover, the T-shaped waveguide does not change the PCNC structure and keeps the interference condition in the PCNC undisturbed, so the discrete resonant modes have no additional phase shift. Therefore, the phase difference between the discrete and continuous modes is no longer an integer multiple of 2π, resulting in an asymmetric transmission spectrum and achieving Fano resonance. The transmittance spectrum can be represented by Eq.(9), and its transmission spectrum is shown in Fig.2.

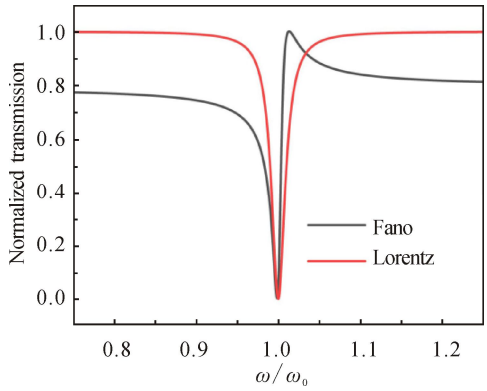

Fig.2 Lorentz line shape and Fano line shape spectra

$$-\mathrm{i}\omega A = -\mathrm{i}\omega_0 A - A\tau_r \mathrm{e}^{-\mathrm{j}\theta} - A\tau_a + \sqrt{2\tau_r \mathrm{e}^{-\mathrm{j}\theta}}S_{I+}, \tag{6}$$

$$S_{I-} = S_{I+} - \sqrt{2\tau_r \mathrm{e}^{-\mathrm{j}\theta}}A, \tag{7}$$

$$S_{R-} = \sqrt{2\tau_a}A, \tag{8}$$

$$T(\omega) = \left|\frac{S_{I-}}{S_{I+}}\right|^2 = \left|\frac{j(\omega-\omega_0) - \tau_r \mathrm{e}^{-\mathrm{j}\theta} + \tau_a}{j(\omega-\omega_0) + \tau_r \mathrm{e}^{-\mathrm{j}\theta} + \tau_a}\right|^2. \tag{9}$$

The device structure proposed in this article is based on a silicon-on-insulator (SOI) platform, which has advantages such as small size and strong scalability compared to other materials such as the SiN platform. The specific structure includes a 700 μm substrate silicon, a 3 μm buried oxide layer, and a 220 nm top silicon layer, as shown in Fig.3(a). The photonic crystal nanobeam and T-shaped bus waveguide are on the top silicon layer, and the waveguide cross-section is shown in Fig.3(b). To achieve single-mode transmission, the waveguide width is set to W_c=W_b=500 nm, as the bus waveguide and nanobeam cavity thickness h are 220 nm. To facilitate process implementation, the coupling distance gap is 200 nm, and the coupling length L_c is 5 μm.

The PCNC comprises a series of circular holes with a gradient radius and a height of h_{hole}=220 nm. According to the Bragg equation a=λ/N_{eff} (using buried oxide layer of SiO_2 and function layer of Si as the materials, N_{eff} is approximately 2.4), when the working wavelength is set

to 1 550 nm and after simulation optimization, the period constant is fixed at a=330 nm.

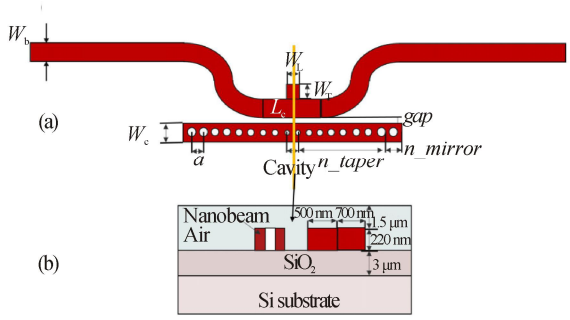

Fig.3 (a) Structure diagram and (b) cross-sectional view of the photonic crystal nanobeam structure

The number of gradient periods of the nanobeam cavity is *n_taper*, and the number of mirror periods is *n_mirror*. The radius of each circular hole gradually increases from 40 nm to 110 nm (with r_{center}=40 nm and r_{end}=110 nm), and the period constant is a=330 nm. The radius of the $r(i)$ circular hole, counted from the middle of the waveguide, can be expressed as

$$r(i)=r_{center}+\frac{i\left(r_{end}-r_{center}\right)}{i_{max}-1}. \tag{10}$$

The Lumerical software based on the 3D FDTD method was used to analyze and optimize the photonic crystal nanobeam. The simulation parameters were kept constant, with the waveguide and nanobeam cavity widths set to W_b=W_c=500 nm, coupling spacing *gap*=200 nm, waveguide T-shaped structure length W_L=700 nm, and width W_T=700 nm. The periodic constant a was set to 330 nm, with a gradient period of *n_taper*=26, and the radius of circular holes was gradually increased from 40 nm to 110 nm. The structure optimization was conducted using the variable control method, where only one parameter was optimized while the other structural parameters were fixed. In this device design, the transmission spectrum of the straight waveguide side-coupled PCNC structure is shown in Fig.4, with an extinction ratio of approximately 7.10 dB and a slope of approximately 3.00 dB/nm. The transmission spectrum of the device with a T-shaped waveguide is also shown in Fig.4. The results show an extinction ratio of 5.51 dB and a 5.86 dB/nm slope. It can be seen that the introduction of the T-shaped waveguide realizes an asymmetric Fano resonance line shape, increasing the spectral resolution by 2.86 dB/nm, while reducing the extinction ratio by only 1.24 dB. Therefore, simulation optimization was performed on the photonic crystal nanobeam with the introduction of the T-shaped waveguide to achieve a high spectral resolution and non-interference photonic device.

To improve the extinction ratio and slope of the photonic crystal nanobeam Fano resonance, optimization was performed on the gradient period number *n_taper* and mirror period number *n_mirror* in the nanobeam cavity. *n_taper* was increased from 18 to 30. The results showed that the transmission spectrum of the photonic crystal nanobeam and the resonant wavelength value changed with the gradient period number *n_taper*, as shown in Fig.5. As *n_taper* increased, the extinction ratio gradually increased and the wavelength experienced a red shift. When *n_taper* was greater than 28, the intensity of the transmission spectrum remained at approximately −8.59 dB. As the number of *n_taper* increases, the optical path length in the PCNC increases. This modification enhances the resonance of the PCNC and increases light absorption, ultimately leading to a higher extinction ratio and slope. Considering the compactness of the structure size, *n_taper*=28 was selected in this paper.

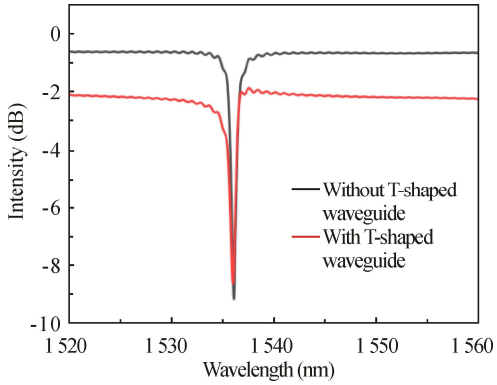

Fig.4 Transmission spectra of photonic crystal nanobeams with and without T-shaped waveguide

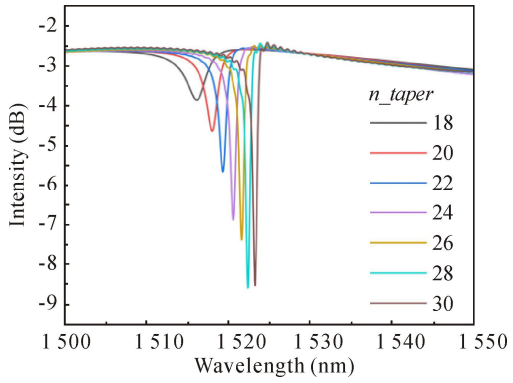

Fig.5 Transmission spectra of photonic crystal nanobeams and the resonant wavelength with different gradient period numbers

Fig.6 shows the relationship between the mirror period number *n_mirror* and minimum light intensity value of transmission spectrum. With a gradient period number *n_taper* of 28, the number of mirror period number *n_mirror* was increased from 0 to 6. The results showed that the intensity reached a minimum when *n_mirror* was 1. At this time, the total number of periods was 29, the intensity was −9.53 dB, the extinction ratio was 7.67 dB, and the slope was 9.47 dB/nm. As the number of *n_mirror* increases, the reflectivity and resonance of the PCNC are enhanced, it was increased the extinction ratio. However,

if *n_mirror* is too large, the losses would also increase, leading to a decrease in the extinction ratio.

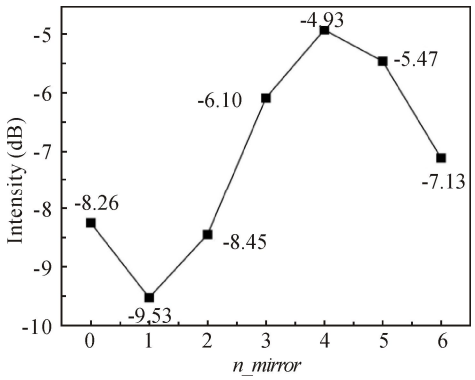

Fig.6 Relationship between mirror period number *n_mirror* and the minimum light intensity of transmission spectrum

To study the effect of the T-shaped waveguide size on the transmission spectrum, this section sets the length of the T-shaped waveguide to W_L=700 nm and changes its width W_T from 500 nm to 900 nm while keeping other parameter values unchanged, as shown in Fig.7. The results show that as the width of the T-shaped waveguide increases, the Fano line shape effect becomes more prominent, and the insertion loss increases. As W_T increases, the optical path increases, leading to a larger insertion loss and an increased slope. When W_T=800 nm, the slope and extinction ratio tend to stabilize. Considering structural size and insertion loss issues, this paper chooses W_T=800 nm as the parameter value for subsequent simulations.

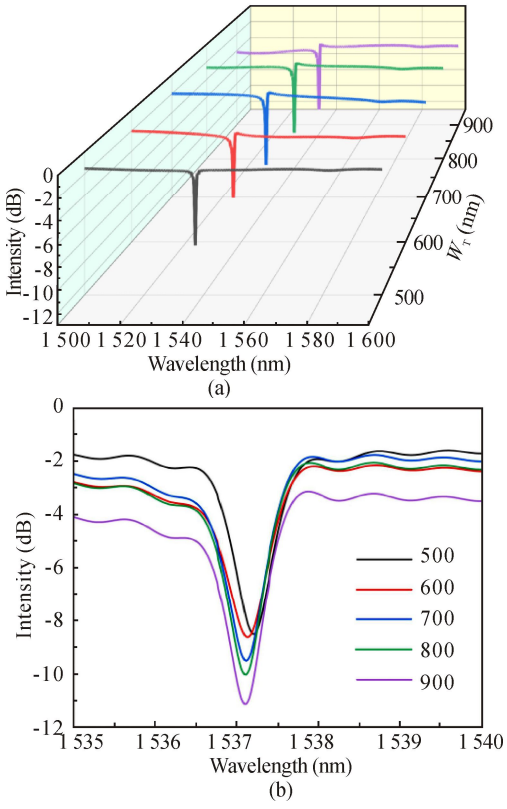

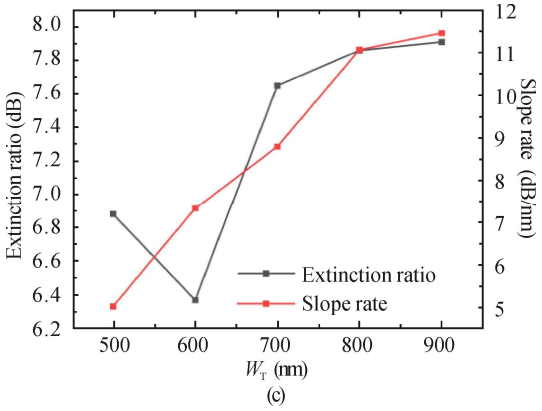

Fig.7 (a) Transmission spectra, (b) spectral comparison, and (c) extinction ratio and slope of devices with different W_T

Fig.8 shows that with the parameter W_T fixed at 800 nm, only the T-shaped waveguide length W_L was varied from 500 nm to 900 nm. When W_L=600 nm, the slope and extinction ratio of the transmission spectrum reached optimal values of 8.7 dB/nm and 11.30 dB, respectively.

Through the above analysis and comparison, it can be concluded that the optimal spectral parameters of the device are *n_taper*=28, *n_mirror*=1, W_T=800 nm, and W_L=600 nm, with an *FSR* of no less than 100 nm. As a convolutional pool, the optical power can be tuned from logical "0" to logical "1" within 0.77 nm, and the multiplexing flux can reach 129, which is 4.3 times higher than the current micro-ring resonator scheme whose

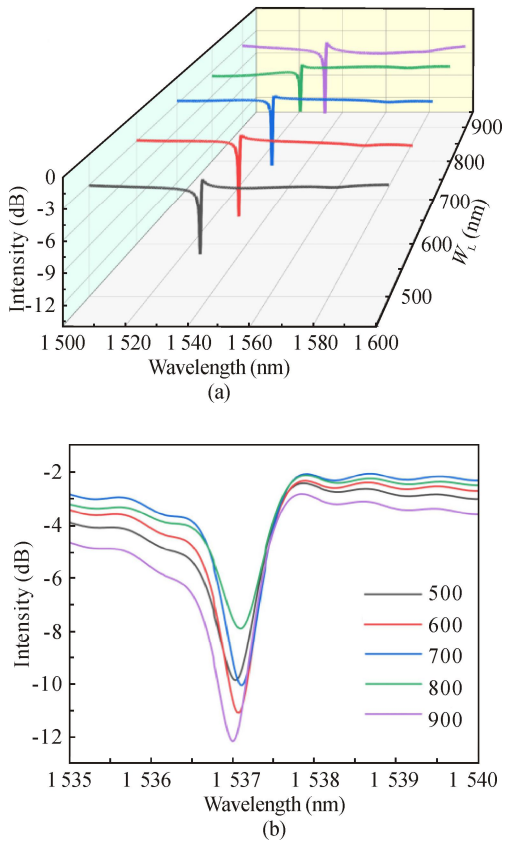

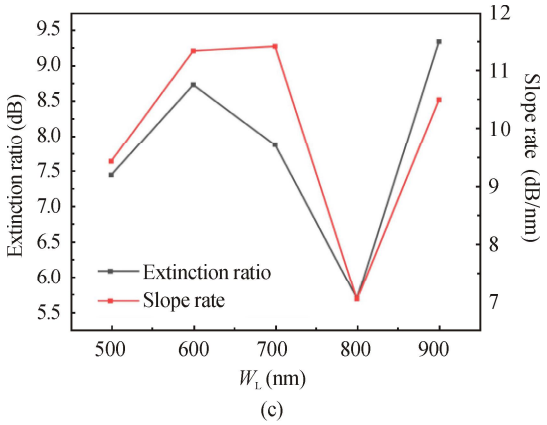

Fig.8 (a) Transmission spectra, (b) spectral comparison, and (c) extinction ratio and slope of devices with different W_L

multiplexing flux is less than or equal to 30, as shown in Tab.1. Compared to other devices, our device exhibits excellent *FSR* and multiplexing flux.

Tab.1 Comparation of different silicon waveguide units for resonance

Structure	*FSR* (nm)	Size (μm^2)	*SR* (dB/nm)	Mux. flux	Ref.
PCNC	-	~8	10	-	[12]
MRR	1.3	~70 650	274.4	~30	[15]
MRR-Fano	~10	~315	26.23	~25	[16]
PCNC-Fano	100	~9	11.30	~129	This work

This paper proposes a compact Fano resonator consisting of a T-shaped waveguide and a PCNC coupler. By introducing a rectangular waveguide on the bus waveguide to introduce phase, the phase difference between the discrete and continuous modes is no longer an integer multiple of 2π, realizing the Fano resonance line shape. The PCNC taper number, mirror period number, and the width and length of the T-shaped waveguide significantly impact the transmission spectrum of the device. The optimal parameters can be obtained when *n_taper*=28, *n_mirror*=1, W_T=800 nm, and W_L=600 nm, with a slope of 8.7 dB/nm and an extinction ratio of 11.30 dB. This Fano resonant structure has no *FSR* within the wavelength ranging from 1 500 nm to 1 600 nm, which can avoid crosstalk and has a high spectral resolution, making it suitable for high-performance photonic devices. Therefore, this compact Fano resonator has high integration and flexibility and can provide a compact fundamental component for future photonic chips, especially in photonic convolutional acceleration computing.

Ethics declarations

Conflicts of interest

The authors declare no conflict of interest.

References

[1] HUANG Y, HUANG B, CHENG C, et al. Feature extraction from images using integrated photonic convolutional kernel[J]. IEEE photonics journal, 2022, 14(3): 1-7.

[2] ANGARI V, MARQUEZ B A, MILLER H, et al. Digital electronics and analog photonics for convolutional neural networks (DEAP-CNNs)[J]. IEEE journal of selected topics in quantum electronics, 2019, 26(1): 1-13.

[3] MILLER D A B. Attojoule optoelectronics for low-energy information processing and communications[J]. Journal of lightwave technology, 2017, 35(3): 346-396.

[4] KRIZHEVSKY A, SUTSKEVER I, HINTON G. ImageNet classification with deep convolutional neural networks[J]. Advances in neural information processing systems, 2012, 25(2).

[5] PRUCNAL P R, BHAVIN J S. Neuromorphic photonics[M]. Boca Raton: CRC press, 2017.

[6] ISHIO H, MINOWA J, NOSU K. Review and status of wavelength-division-multiplexing technology and its application[J]. Journal of lightwave technology, 1984, 2(4): 448-463.

[7] DING X, WU G, ZUO F, et al. Bidirectional optical amplifier for time transfer using bidirectional WDM transmission[J]. Optoelectronics letters, 2019, 15(6): 401-405.

[8] HINAKURA Y, AKIYAMA D, ITO H, et al. Silicon photonic crystal modulators for high-speed transmission and wavelength division multiplexing[J]. IEEE journal of selected topics in quantum electronics, 2020, 27(3): 1-8.

[9] DONG P. Silicon photonic integrated circuits for wavelength-division multiplexing applications[J]. IEEE journal of selected topics in quantum electronics, 2016, 22(6): 370-378.

[10] LIU W, LIU W, YE Y, et al. Holylight: a nanophotonic accelerator for deep learning in data centers[C]//2019 Design, Automation & Test in Europe Conference & Exhibition (DATE), March 25-29, 2019, Florence, Italy. New York: IEEE, 2019: 1483-1488.

[11] JHA A, HUANG C, DELIMA T F, et al. Nanophotonic cavity based synapse for scalable photonic neural networks[J]. IEEE journal of selected topics in quantum electronics, 2022, 28(6): 1-8.

[12] GU L, WANG B, YUAN Q, et al. Fano resonance from a one-dimensional topological photonic crystal[J]. APL photonics, 2021, 6(8): 086105.

[13] MENG Z M, LIANG A, LI Z Y. Fano resonances in photonic crystal nanobeams side-coupled with nanobeam cavities[J]. Journal of applied physics, 2017, 121(19): 193102.

[14] XU W, ZHU Z H, LIU K, et al. Chip-integrated nearly perfect absorber at telecom wavelengths by graphene coupled with nanobeam cavity[J]. Optics letters, 2015, 40(14): 3256-3259.

[15] YU H, QIU F. Compact thermo-optic modulator based on a titanium dioxide micro-ring resonator[J]. Optics letters, 2022, 47(8): 2093-2096.

[16] XU Y, LU L, CHEN G, et al. T-shaped silicon waveguide coupled with a micro-ring resonator-based Fano resonance modulator[J]. Applied optics, 2022, 61(31): 9217-9224.